

We are IntechOpen, the world's leading publisher of Open Access books Built by scientists, for scientists

6,900

Open access books available

186,000

International authors and editors

200M

Downloads

Our authors are among the

154

Countries delivered to

TOP 1%

most cited scientists

12.2%

Contributors from top 500 universities



WEB OF SCIENCE™

Selection of our books indexed in the Book Citation Index
in Web of Science™ Core Collection (BKCI)

Interested in publishing with us?
Contact book.department@intechopen.com

Numbers displayed above are based on latest data collected.
For more information visit www.intechopen.com



Effect of Turbulence on Fixed-Speed Wind Generators

Hengameh Kojooyan Jafari

Additional information is available at the end of the chapter

<http://dx.doi.org/10.5772/51407>

1. Introduction

The influence of wind energy connection to the grid has increased greatly and turbulence or unreliable characteristics of wind energy are expected to produce frequency and voltage changes in power systems and protection system equipment. To prevent these changes, it is necessary to study the working point change due to turbulence. In other papers, the voltage and transient stability analysis have been studied during and after turbulence [2] and the impact of WTGs (wind turbine generators) on the system frequency, inertia response of different wind turbine technologies, and comparison between inertia response of single-fed and doubly-fed induction generators have been examined. Moreover study of the frequency change alone was conducted using Dig-SILENT simulator for FSWTs (fast-speed wind turbines) with one-mass shaft model [2].

In this chapter both frequency and grid voltage sag change are presented with MATLAB analytically and also by SIMULINK simulation in FSWTs with one- and two-mass shaft turbine models to compare both results and a new simulation of induction machine without limiter and switch blocks is presented as a new work. The first part of study is frequency change effect on wind station by SIMULINK that shows opposite direction of torque change in comparison with previous studies with Dig-SILENT. The second part of study is effect of frequency and voltage sag change on wind station torque due to turbulence in new simulation of induction generator that is new idea.

2. Wind turbine model

The equation of wind turbine power is

$$P = \frac{1}{2} \rho A C_p v_w^3 \tag{1}$$

where ρ is air density, A is area of turbine, C_p is power coefficient and v_w is wind speed.

The C_p curve and equation are shown in Fig. 1 and given by equation (2) and (3)

$$C_p = c_1 \left(c_2 \frac{1}{\left(\frac{1}{\lambda + c_8 \theta_{pitch}} - \frac{c_9}{1 + \theta_{pitch}^3} \right)} - c_3 \theta_{pitch} - c_4 \theta_{pitch}^5 - c_6 \right) e^{-c_7 \left(\frac{1}{\lambda + c_8 \theta_{pitch}} - \frac{c_9}{1 + \theta_{pitch}^3} \right)} \tag{2}$$

$$C_p = 0.44 \left(125 \left(\frac{1}{\lambda} + 0.002 \right) - 6.94 \right) \cdot e^{-16.5 \left(\frac{1}{\lambda} + 0.002 \right)} \tag{3}$$

where θ_{pitch} is blade pitch angle, λ is the tip speed ratio described by equation (4). The parameters are given in Table 1.

$$\lambda = \frac{\omega_M R}{v_w} \tag{4}$$

where R is blade radius.

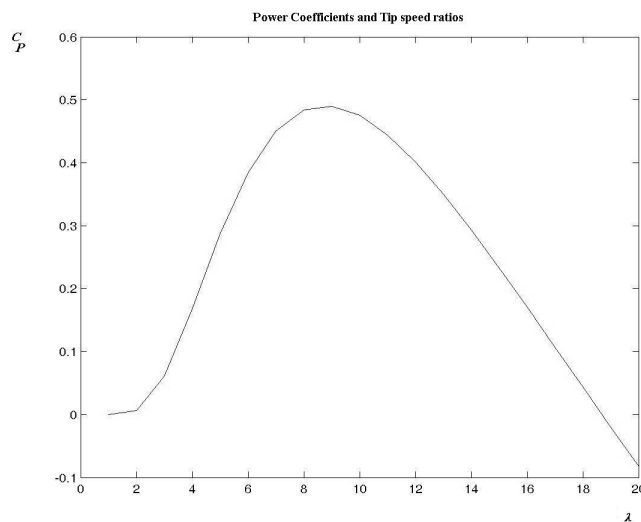


Figure 1. Curve of C_p for different tip speed ratios λ .

The curve of Fig.1 has positive slope before $C_{p \max}$ and it has negative slope after $C_{p \max}$.

3. One-Mass Shaft Wind Station Model

Induction machine equation is

$$T_e - T_m = J \frac{d\omega_m}{dt} + C\omega_m \quad (5)$$

Where, T_m is the mechanical torque, T_e is the generator torque, C is the system drag coefficient and J is the total inertia.

Table 1 shows the parameters of the one-mass shaft turbine model and induction generator.

Generator	Wind Turbine
$R_s = .011\Omega$	$c_1 = .44$
$L_s = .000054H$	$c_2 = 125$
$L_m = .00287H$	$c_3 = 0$
$L'_r = .000089H$	$c_4 = 0$
$R'_r = .0042 [\Omega]$	$c_5 = 0.1$
$J_m = .5 \text{ to } 20.26 [\text{kgm}^2]$	$c_6 = 6.94$
$p(\# \text{pole pairs}) = 2$	$c_7 = 16.5$
$P_n = 2e6 [w]$	$c_8 = 0.1$
	$c_9 = -.002$
	$R = 35 [m]$
	$A = \pi R^2 [m^2]$
	$\rho = 1.2041 [\text{kg}/m^3]$
	$v_w = 6, 10, 13 [m/s]$
	$\theta_{pitch} = 0 [^\circ]$

Table 1. Parameters of one- mass shaft turbine model and generator.

4. Two-Mass Shaft Induction Machine Model

This model is used to investigate the effect of the drive train or two-mass shaft, i.e., the masses of the machine and the shaft, according to the equation (8) [3], [4]. In this equation, J_t is wind wheel inertia, J_G is gear box inertia and generator's rotor inertia connected through

the elastic turbine shaft with a κ as an angular stiffness coefficient and C as an angular damping coefficient.

The angular shaft speed ω_t can be obtained from equations (6) and (7) [1], [3], [4].

T_G is the torque of the machine, T_t is the turbine torque, δ_t is the angular turbine shaft angle, δ_G is the angular generator shaft angle, ν is the inverse of the gear box ratio and J_G and J_t are the inertia of the machine shaft and turbine shaft, respectively.

The Parameters, defined above, are given in Table 2.

This model is described as equation (8).

$$T_G = J_G \frac{d\omega_G}{dt} - \frac{\kappa}{\nu} (\delta_t - \delta_{GB}) - \frac{C}{\nu} (\omega_t - \omega_{GB}) \quad (6)$$

$$T_t = J_t \frac{d\omega_t}{dt} + \kappa (\delta_t - \delta_{GB}) + C (\omega_t - \omega_{GB}) \quad (7)$$

$$\begin{pmatrix} \dot{\omega}_G \\ \dot{\omega}_t \\ \omega_G \\ \omega_t \end{pmatrix} = \begin{pmatrix} \frac{-\nu^2 \cdot C}{J_G} & \frac{-\nu \cdot C}{J_G} & \frac{-\nu^2 \cdot \kappa}{J_G} & \frac{\nu \kappa}{J_G} \\ \frac{\nu \cdot C}{J_t} & \frac{-C}{J_t} & \frac{-\nu \kappa}{J_t} & \frac{-\kappa}{J_t} \\ 1 & 0 & 0 & 0 \\ 0 & 1 & 0 & 0 \end{pmatrix} \begin{pmatrix} \omega_G \\ \omega_t \\ \delta_G \\ \delta_t \end{pmatrix} + \begin{pmatrix} \frac{1}{J_G} & 0 \\ 0 & \frac{1}{J_t} \\ 0 & 0 \\ 0 & 0 \end{pmatrix} \begin{pmatrix} T_G \\ T_t \end{pmatrix} \quad (8)$$

ν	1/80
J_G [kg.m ²]	.5
J_t [kg.m ²]	1
C [Nm/rad ²]	1e6
κ [Nm/rad]	6e7

Table 2. Parameters of two-mass shaft model.

5. Induction Machine and Kloss Theory

In a single-fed induction machine, the torque angular speed curve of equation (12) [1] is nonlinear, but by using the Kloss equation (13), equations (9), (10), and (11), this curve is linearly modified [1], [2] as shown in Fig. 2. Therefore, the effect of frequency changes in wind power stations can be derived precisely by equation (12) and approximately using equation (13), as shown in Figs. 2–6.

$$G = \pm \sqrt{\frac{\left(\frac{f_s}{f_b}\right)^{-2} R_s^2 + X_{ss}^2}{\left(X_m^2 - X_{ss} X'_{rr}\right)^2 \left(\frac{f_s}{f_b}\right)^2 + R_s^2 X'_{rr}{}^2}} \quad (9)$$

$$s_k = R'_r G \quad (10)$$

$$T_k = \frac{\frac{f_s}{f_b} X_m^2 G V_s^2}{\left(R_s + G \left(\frac{f_s}{f_b}\right)^2 \left(X_m^2 - X_{ss} X'_{rr}\right)\right)^2 + \left(\frac{f_s}{f_b}\right)^2 \left(X_{ss} + G R_s X'_{rr}\right)^2} \quad (11)$$

$$T_e = \frac{\frac{f_s}{f_b} X_m^2 R'_r V_s^2}{\left(R_s + G \left(\frac{f_s}{f_b}\right)^2 \left(X_m^2 - X_{ss} X'_{rr}\right)\right)^2 + \left(\frac{f_s}{f_b}\right)^2 \left(X_{ss} + G R_s X'_{rr}\right)^2} \quad (12)$$

$$T_e = 2T_k \frac{s}{s_k}; s \ll s_k \quad (13)$$

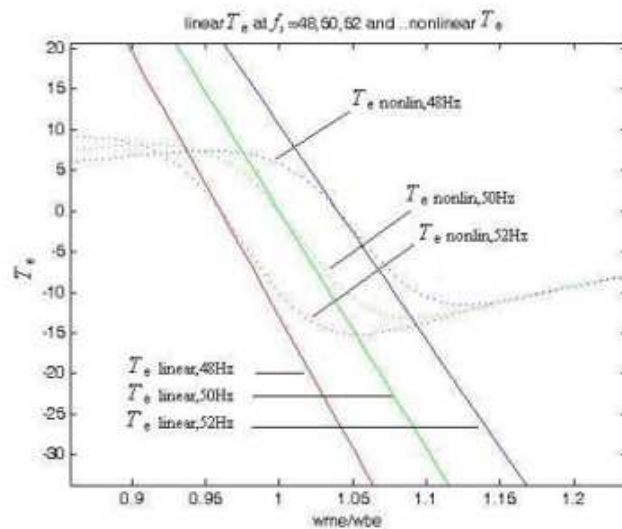


Figure 2. Electrical torque (nonlinear and linear) versus speed (slip).

Equations (11) and (12) are given in per unit, but the associated resistances are in ohms.

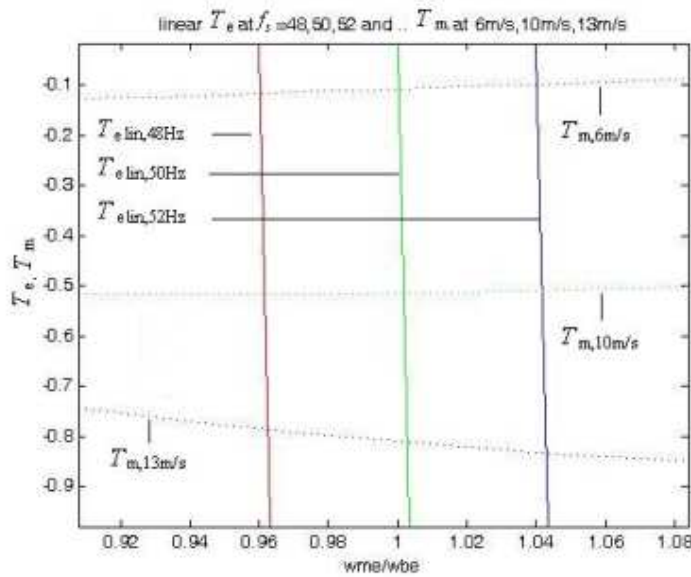


Figure 3. Mechanical and linear electrical torque versus slip.

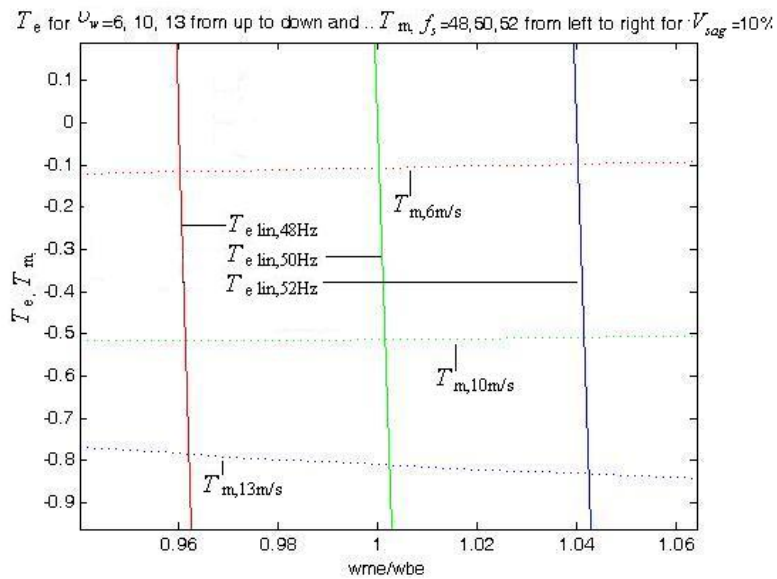


Figure 4. Mechanical and electrical torque versus frequency curves per unit with $V_{sag} = 10\%$.

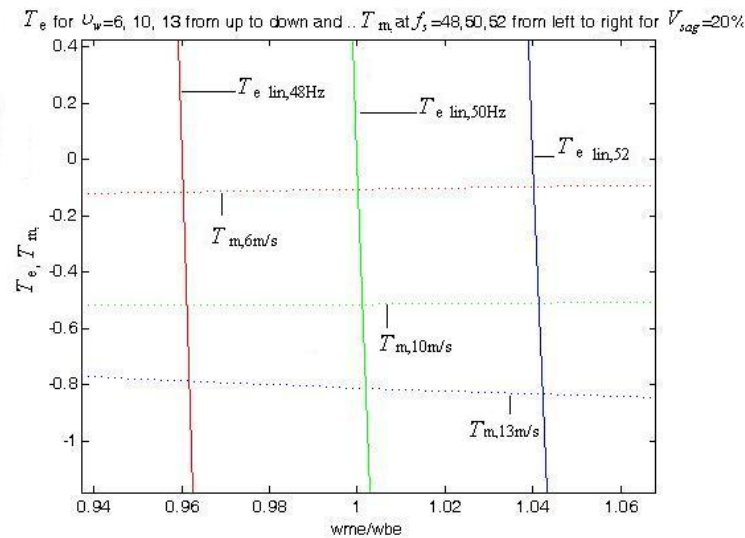


Figure 5. Mechanical and electrical torque versus frequency per unit with $V_{\text{sag}} = 20\%$.

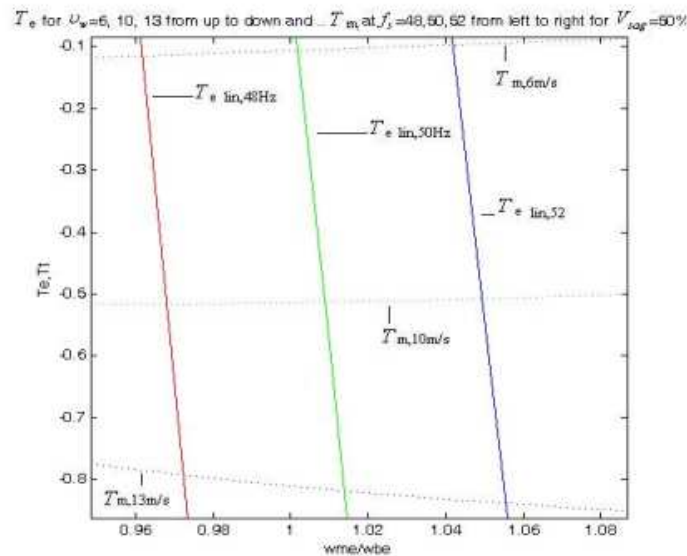


Figure 6. Mechanical and electrical torque versus frequency per unit with $V_{\text{sag}} = 50\%$.

Figs. 3, 4, 5, and 6 illustrate that for lower wind speeds of 6 and 10 m/s, as the synchronous frequency f_s and V_{sag} change, the T_e and T_m values of the rotor change in the same direction as the frequency of the network, as shown in Tables III, IV, V, and VI. These figures and tables give the results for $V_{\text{sag}} = 0\%$ (i.e., only the frequency changes), 10%, 20%, and 50%. However, for a higher wind speed of 13 m/s, as f_s and V_{sag} change, the T_e and T_m values of the rotor change in the opposite direction to the changes in the frequency of the network.

For small changes in the slip according to the Kloss approach in equation (13), the torque changes as follows [2]:

$$T_{m1} = T_{m0} + K_{\alpha} \Delta\omega \quad (14)$$

Then:

$$T_{m1} = 2 \frac{T_k}{s_k} \left(1 - \frac{\omega_{m0} + \Delta\omega}{\omega_e} \right) \quad (15)$$

and

$$K_{\alpha} = \frac{\partial T}{\partial \omega} = \frac{\partial T}{\partial \lambda} \cdot \frac{\partial \lambda}{\partial \omega} \quad (16)$$

or

$$K_{\alpha} = \frac{1}{\omega_{M0}} \left(\frac{1}{2} \rho R^4 v_{\omega 0} \frac{\partial C_p}{\partial \lambda} \Big|_{\lambda_0, v_0} - T_{M0} \right) \quad (17)$$

Thus, the new angular operation speed[2] is

$$\Delta\omega = \frac{-T_{m0} + 2 \frac{T_k}{s_k} - 2 \frac{T_k}{s_k} \frac{\omega_{m0}}{\omega_e}}{k_{\alpha} + 2 \frac{T_k}{s_k \omega_e}} \quad (18)$$

u_w	$f_s = 48$		$f_s = 50$		$f_s = 52$	
	$\omega_m [pu]$	$T_e [pu]$	$\omega_m [pu]$	$T_e [pu]$	$\omega_m [pu]$	$T_e [pu]$
6	.96050	-.1157	1.0005	-.1064	1.0405	-.0974
10	.9621	-.5337	1.0021	-.491	1.0421	-.4493
13	.9631	-.7863	1.0035	-.8122	1.0439	-.8331

Table 3. Analytical MATLAB results for different frequencies.

u_w	$f_s = 48$		$f_s = 50$		$f_s = 52$	
	$\omega_m[pu]$	$T_e[pu]$	$\omega_m[pu]$	$T_e[pu]$	$\omega_m[pu]$	$T_e[pu]$
6	.9606	-.1156	1.0006	-.1064	1.0406	-.0974
10	.9625	-.5163	1.0027	-.5137	1.0429	-.5086
13	.9738	-.7868	1.0043	-.8127	1.0448	-.8335

Table 4. Analytical MATLAB results for $V_{sag} = 10\%$.

u_w	$f_s = 48$		$f_s = 50$		$f_s = 52$	
	$\omega_m[pu]$	$T_e[pu]$	$\omega_m[pu]$	$T_e[pu]$	$\omega_m[pu]$	$T_e[pu]$
6	.9607	-.1156	1.0007	-.1064	1.0407	-.0974
10	.9632	-.5163	1.0034	-.5136	1.0437	-.5085
13	.9648	-.7875	1.0054	-.8134	1.0461	-.8341

Table 5. Analytical MATLAB results for $V_{sag} = 20\%$

u_w	$f_s = 48$		$f_s = 50$		$f_s = 52$	
	$\omega_m[pu]$	$T_e[pu]$	$\omega_m[pu]$	$T_e[pu]$	$\omega_m[pu]$	$T_e[pu]$
6	.9618	-.1153	1.0018	-.1061	1.0418	-.0971
10	.9681	-.5161	1.0088	-.5131	1.0494	-.5076
13	.9724	-.7927	1.0139	-.8181	1.0555	-.8382

Table 6. Analytical MATLAB results for $V_{sag} = 50\%$

6. Simulation of wind generator with frequency change

During turbulence and changes in the grid frequency, the torque speed (slip) curves change in such a way that as the frequency increases, the torque is increased at low wind speeds; 6 and 10 m/s, in contrast to Fig. 6 and decreases at a high speed of 13 m/s [2], as shown in Table 7 and Figs. 7–15.

u_w	$f_s = 48$		$f_s = 50$		$f_s = 52$	
	$\omega_m[pu]$	$T_e[pu]$	$\omega_m[pu]$	$T_e[pu]$	$\omega_m[pu]$	$T_e[pu]$
6	.9619	-.1148	1.0019	-.1057	1.0418	-.0969
10	.9684	-.5179	1.0091	-.5134	1.0494	-.5076
13	.9724	-.7945	1.0147	-.8177	1.0559	-.8373

Table 7. Simulink simulation results for one- and two-mass shaft models

Figs. 7–15 show the electrical torque and mechanical speed of the induction machine for the one- and two-mass shaft turbine models at wind speeds of 6, 10, and 13 m/s to validate Table 7.

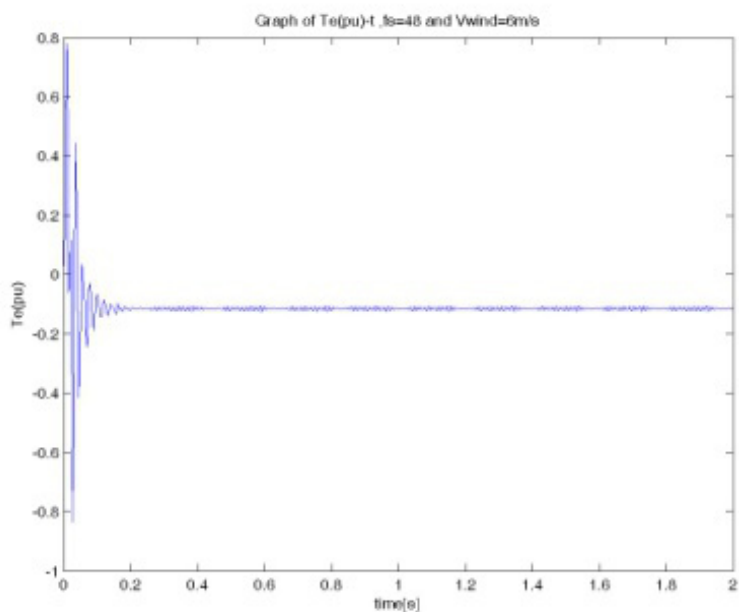


Figure 7. Electrical torque when $f_s = 48$ and $v_w = 6$ m/s.

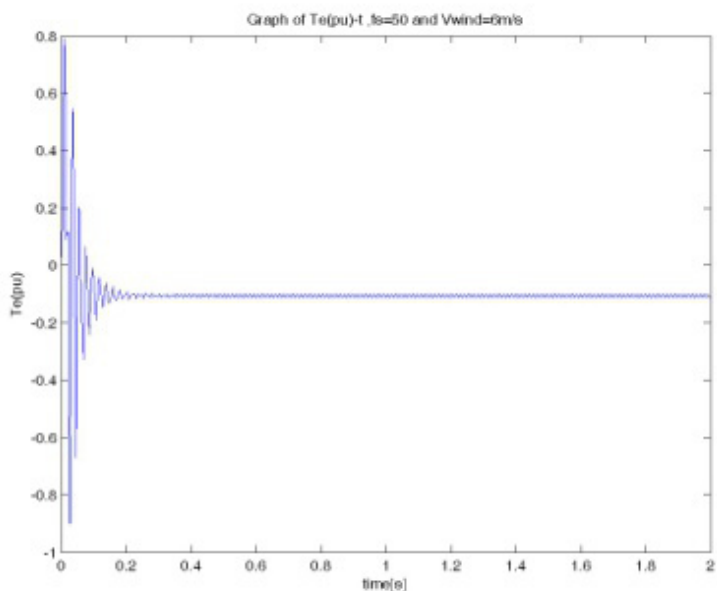


Figure 8. Electrical torque when $f_s = 50$ and $v_w = 6$ m/s.

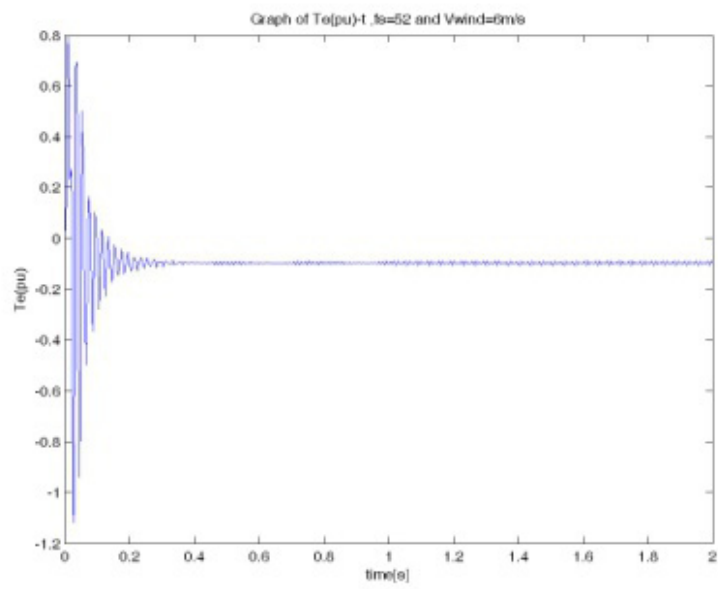


Figure 9. Electrical torque when $f_s = 52$ and $u_w = 6$ m/s.

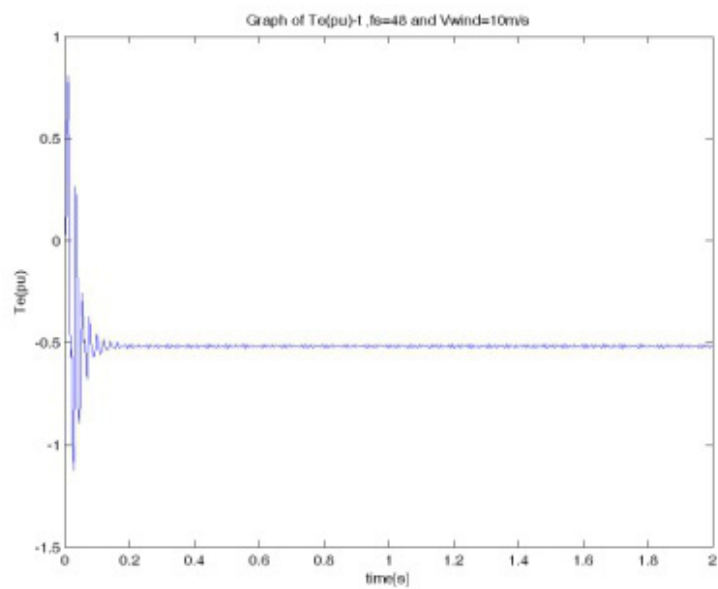


Figure 10. Electrical torque when $f_s = 48$ and $u_w = 10$ m/s.

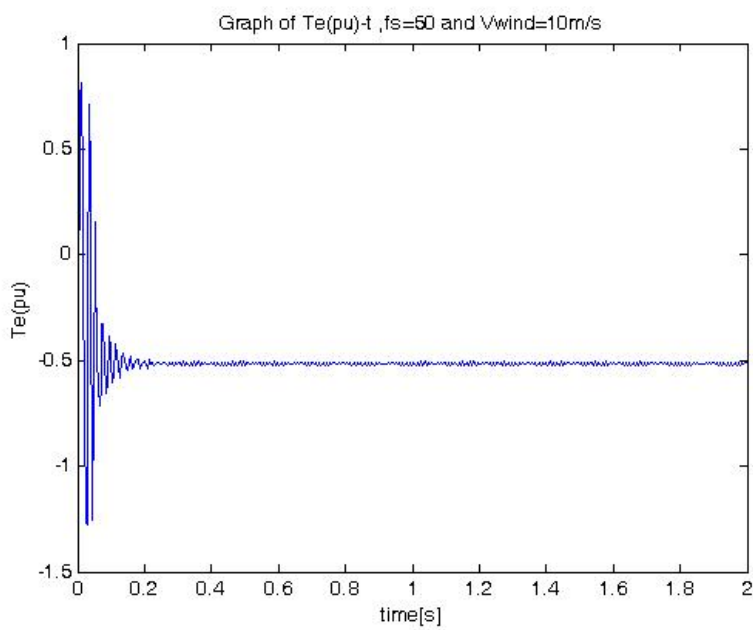


Figure 11. Electrical torque when $f_s=50$ and $u_w=10$ m/s.

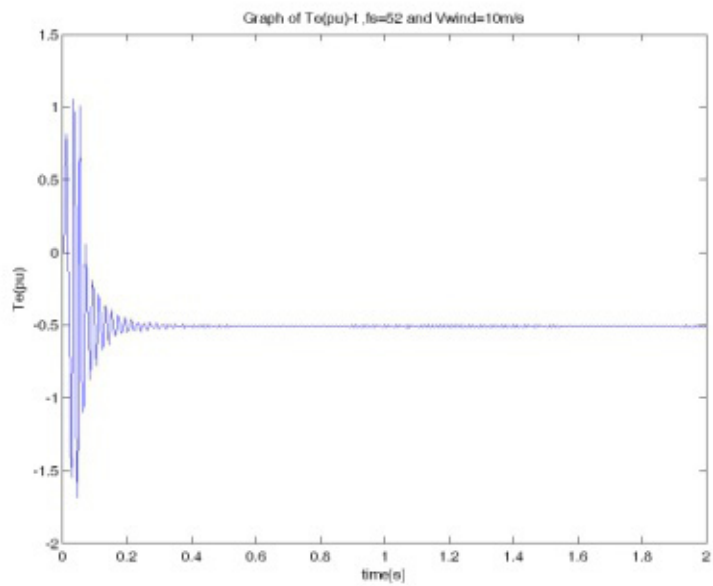


Figure 12. Electrical torque when $f_s=52$ and $u_w=10$ m/s.

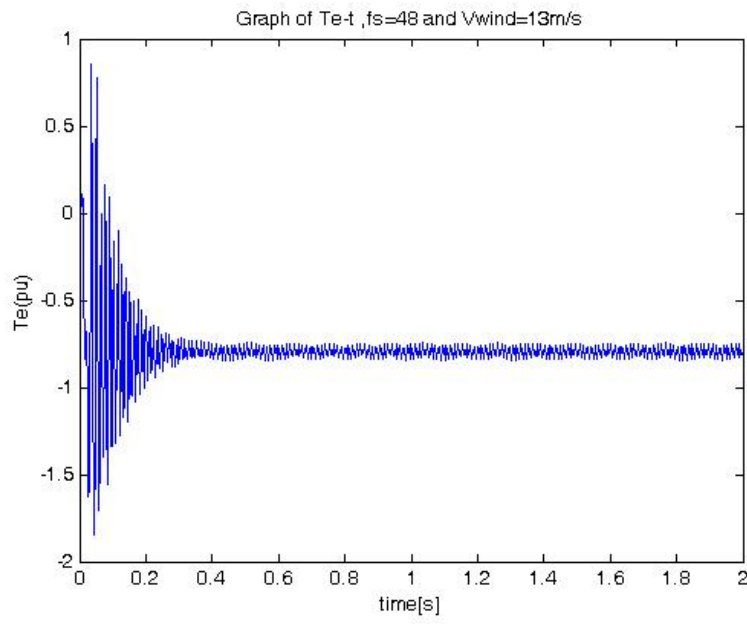


Figure 13. Electrical torque when $f_s = 48$ and $u_w = 13$ m/s.

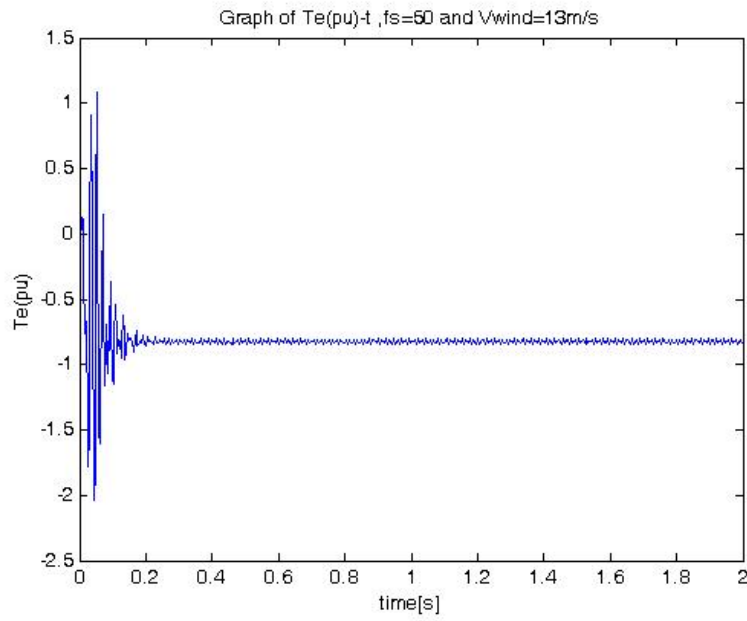


Figure 14. Electrical torque when $f_s = 50$ and $u_w = 13$ m/s.

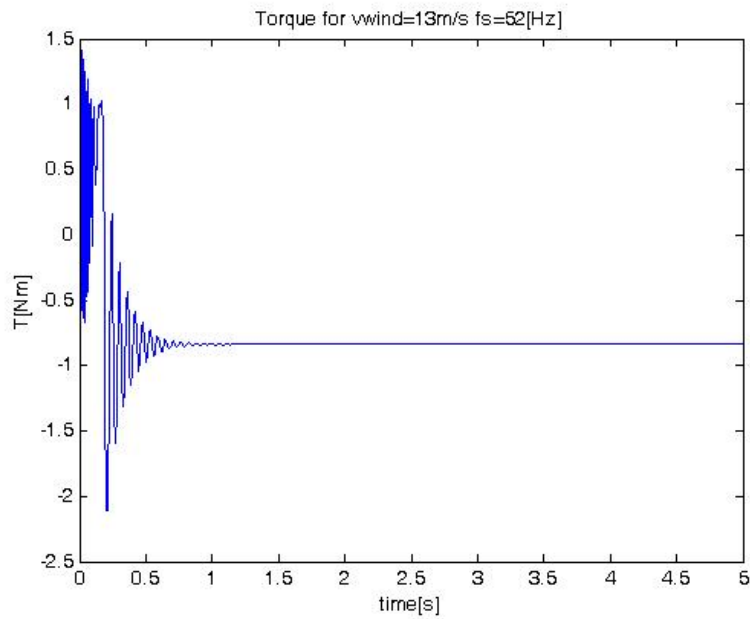


Figure 15. Electrical torque when $f_s=52$ and $u_w=13\text{m/s}$.

7. Simulation of wind station with one-mass and two-mass shaft turbine models

The results of simulations of a simple grid, fixed-speed induction machine, and one-mass and two-mass shaft turbines are given in Tables 8 -10 and Figs. 16–42. For an induction wind generator using the induction block in SIMULINK with high voltage sag i.e. 50% with frequencies 50 and 52 and equal to 13, C_p becomes negative, and the results are unrealistic. Then results of 50% voltage sag are realistic in new simulation of induction machine in Tables 8 -10.

u_w	$f_s=48$		$f_s=50$		$f_s=52$	
	$\omega_m[pu]$	$T_e[pu]$	$\omega_m[pu]$	$T_e[pu]$	$\omega_m[pu]$	$T_e[pu]$
6	.9624	-.1152	1.0024	-.106	1.0423	-.097
10	.9703	-.516	1.0111	-.5128	1.0519	-.5071
13	.9757	-.795	1.0176	-.8201	1.0595	-.8399

Table 8. Simulation results by SIMULINK for one and two mass shaft model for $V_{sag}=10\%$

u_w	$f_s=48$		$f_s=50$		$f_s=52$	
	$\omega_m[pu]$	$T_e[pu]$	$\omega_m[pu]$	$T_e[pu]$	$\omega_m[pu]$	$T_e[pu]$
6	.963	-.1151	1.003	-.1059	1.043	-.0969
10	.973	-.5159	1.014	-.5125	1.055	-.5066
13	.9799	-.7977	1.0223	-.8226	1.0648	-.842

Table 9. Simulation results by SIMULINK for one and two mass shaft model for $V_{sag}=20\%$

u_w	$f_s=48$		$f_s=50$		$f_s=52$	
	$\omega_m[pu]$	$T_e[pu]$	$\omega_m[pu]$	$T_e[pu]$	$\omega_m[pu]$	$T_e[pu]$
6	.9674	-.114	1.0074	-.1048	1.0474	-.0959
10	.9933	-.5146	1.0364	-.5096	1.0796	-.502
13	1.0248	-.8239	1.0474	-.8347	1.0917	-.85

Table 10. Simulation results by SIMULINK for one and two mass shaft model for $V_{sag}=50\%$

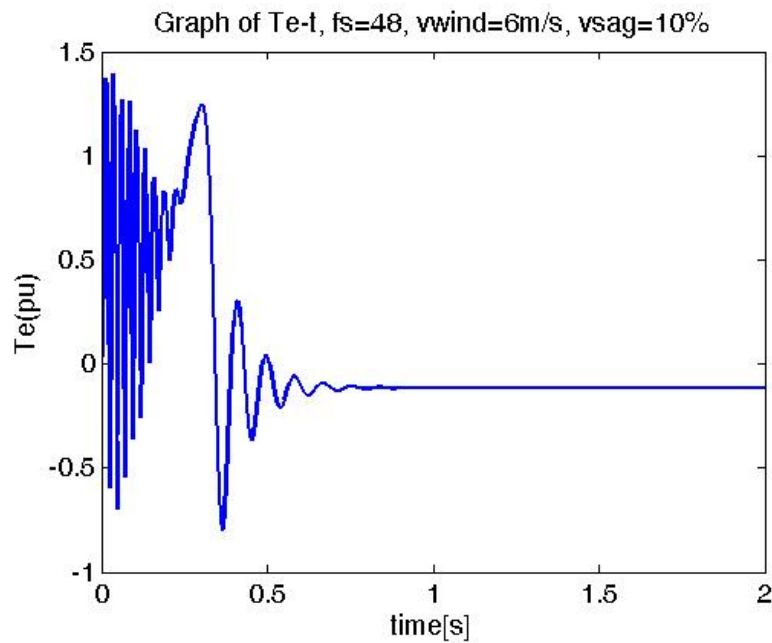


Figure 16. Torque-time in per unit while $V_{sag}=10\%$ and $u_w=6m/s$, $f_s=48$

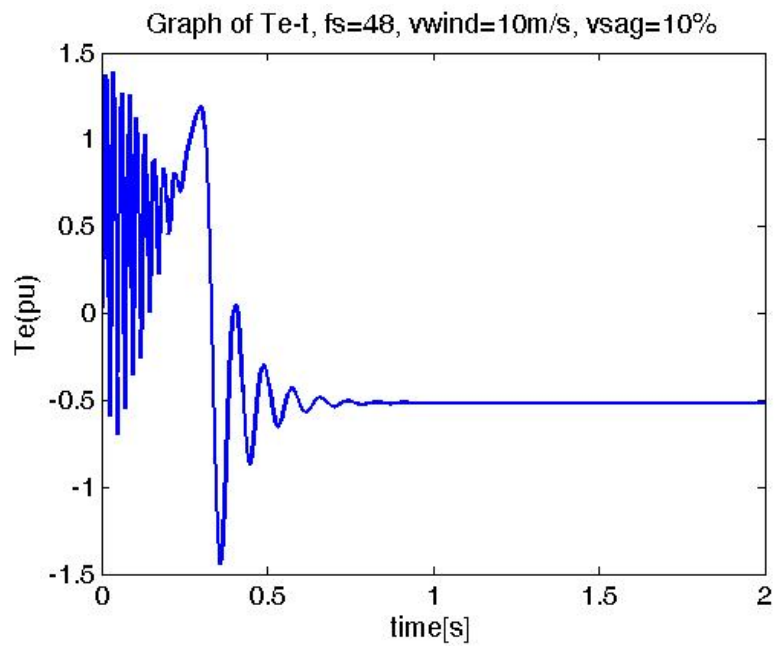


Figure 17. Torque-time in per unit while $V_{sag} = 10\%$ and $u_w = 10\text{m/s}$, $f_s = 48$

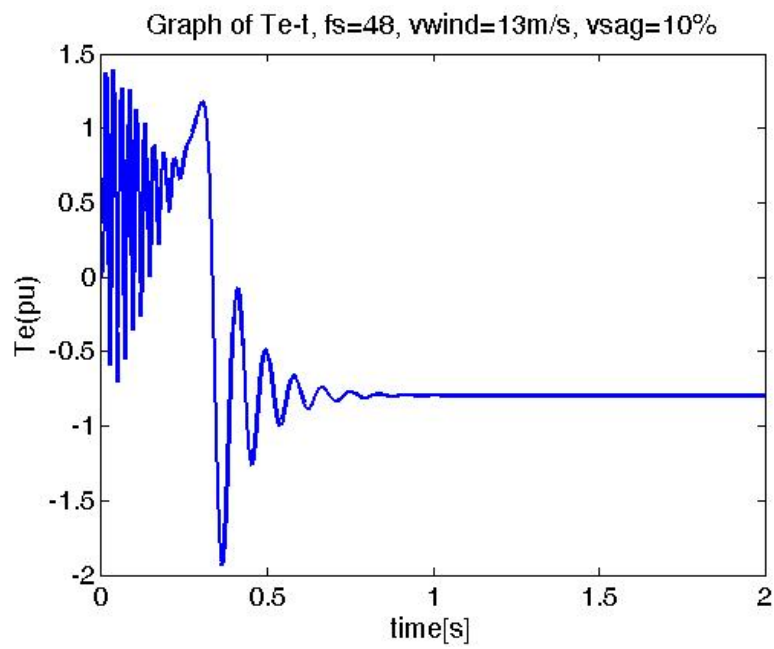


Figure 18. Torque-time in per unit while $V_{sag} = 10\%$ and $u_w = 13\text{m/s}$, $f_s = 48$

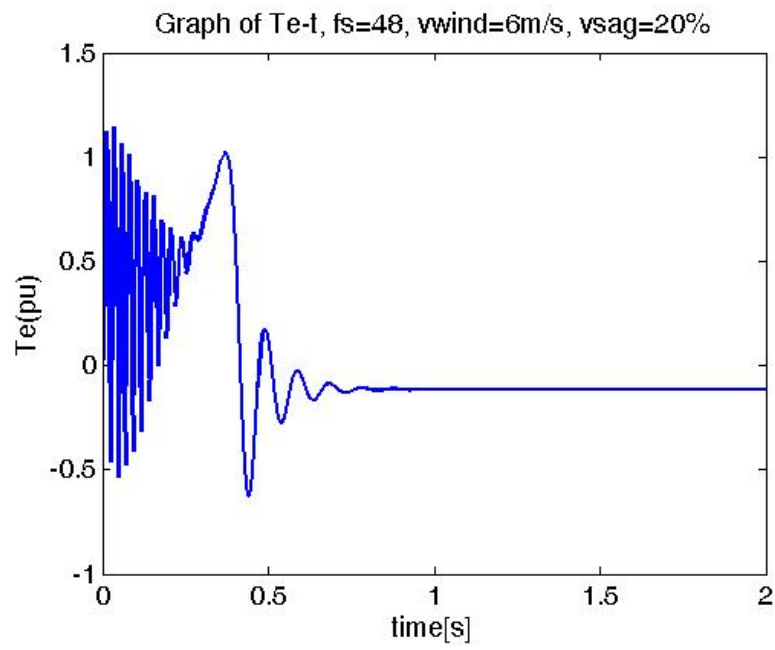


Figure 19. Torque-time in per unit while $V_{sag}=20\%$ and $u_w = 6\text{m/s}$, $f_s = 48$

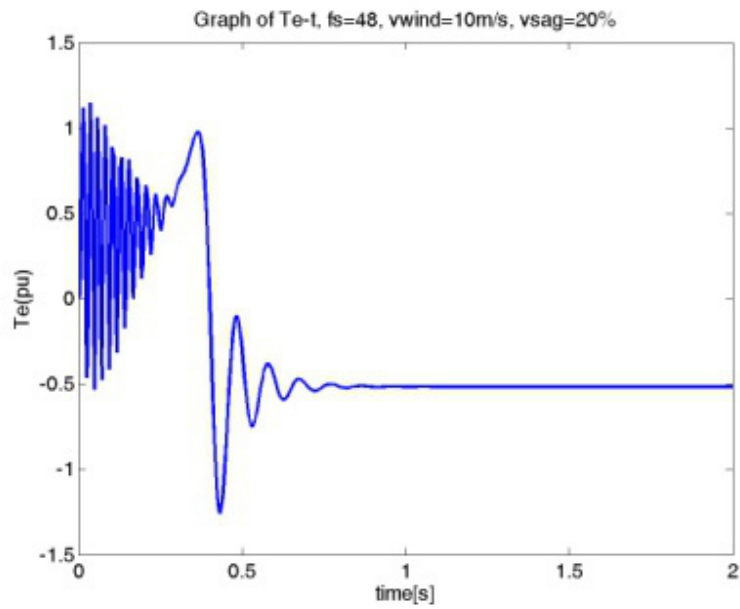


Figure 20. Torque-time in per unit while $V_{sag}=20\%$ and $u_w = 10\text{m/s}$, $f_s = 48$

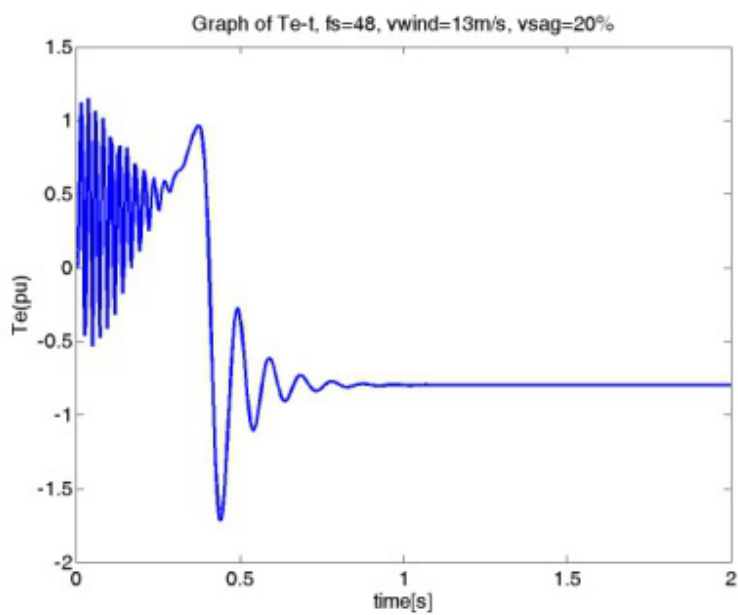


Figure 21. Torque-time in per unit while $V_{sag}=20\%$ and $u_w=13\text{m/s}$, $f_s=48$

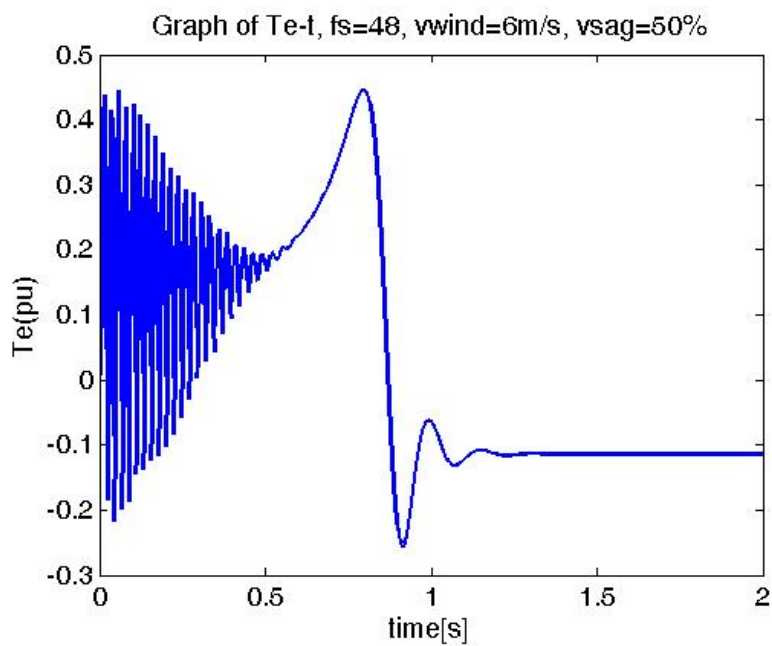


Figure 22. Torque-time in per unit while $V_{sag}=50\%$ and $u_w=6\text{m/s}$, $f_s=48$

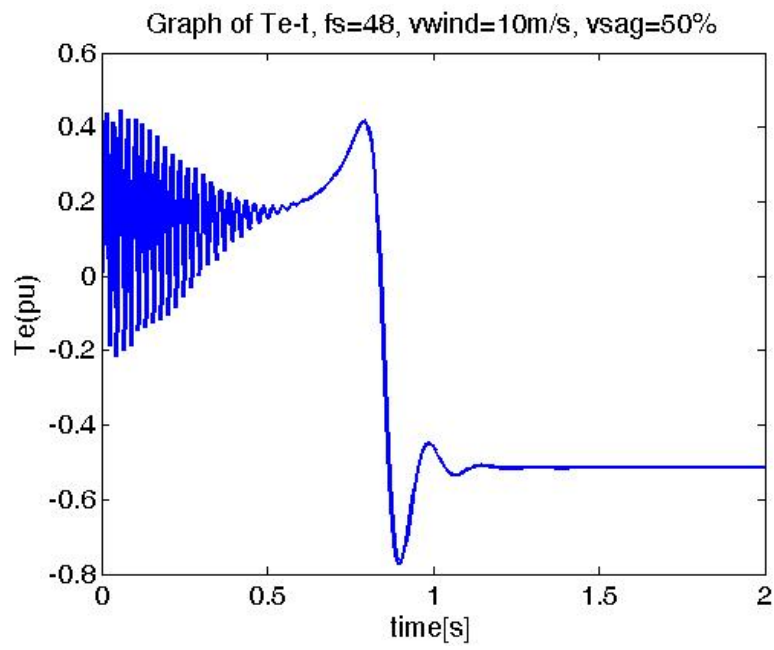


Figure 23. Torque-time in per unit while $V_{sag} = 50\%$ and $u_w = 10\text{m/s}$, $f_s = 48$

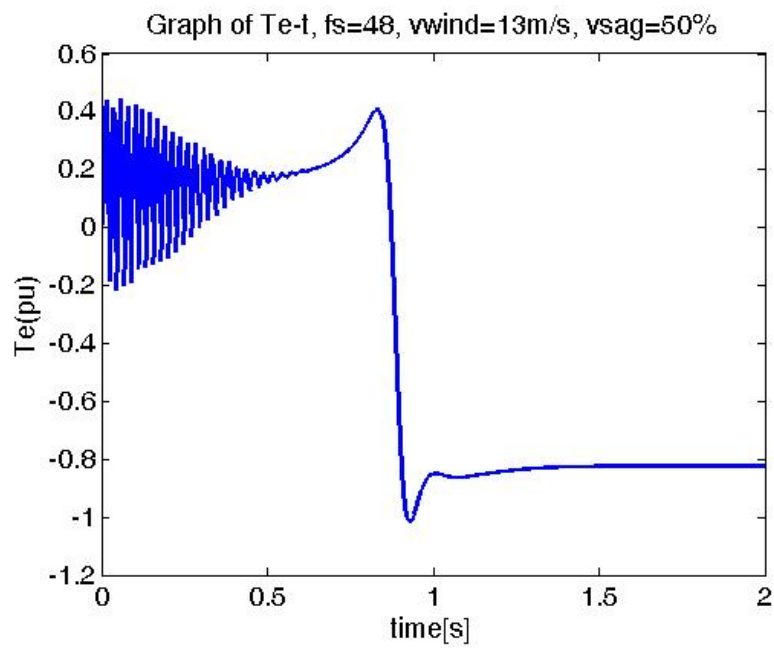


Figure 24. Torque-time in per unit while $V_{sag} = 50\%$ and $u_w = 13\text{m/s}$, $f_s = 48$

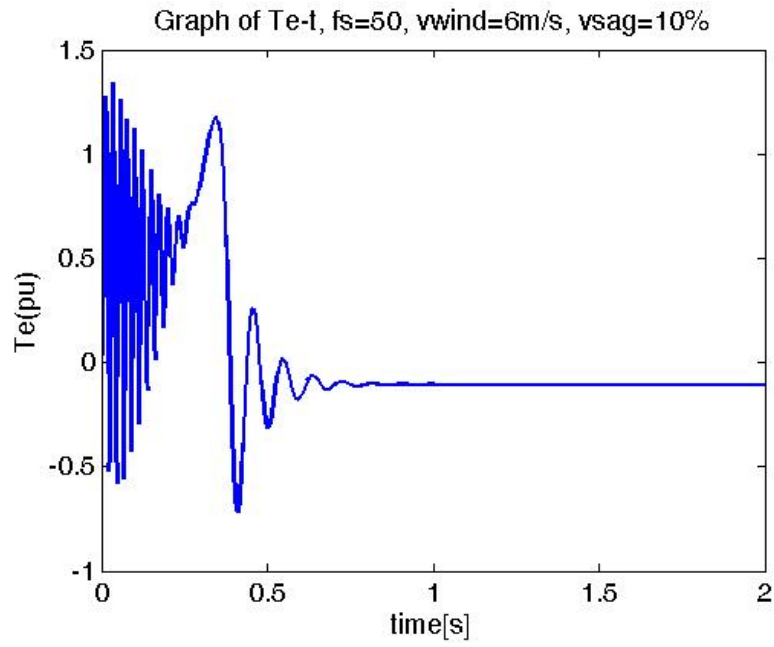


Figure 25. Torque-time in per unit while $V_{sag} = 10\%$ and $u_w = 6\text{m/s}$, $f_s = 50$

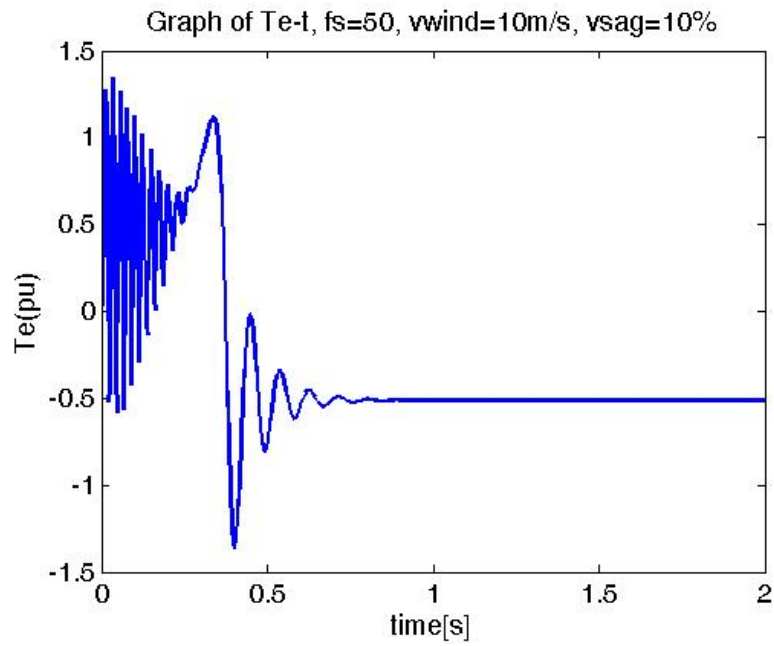


Figure 26. Torque-time in per unit while $V_{sag} = 10\%$ and $u_w = 10\text{m/s}$, $f_s = 50$

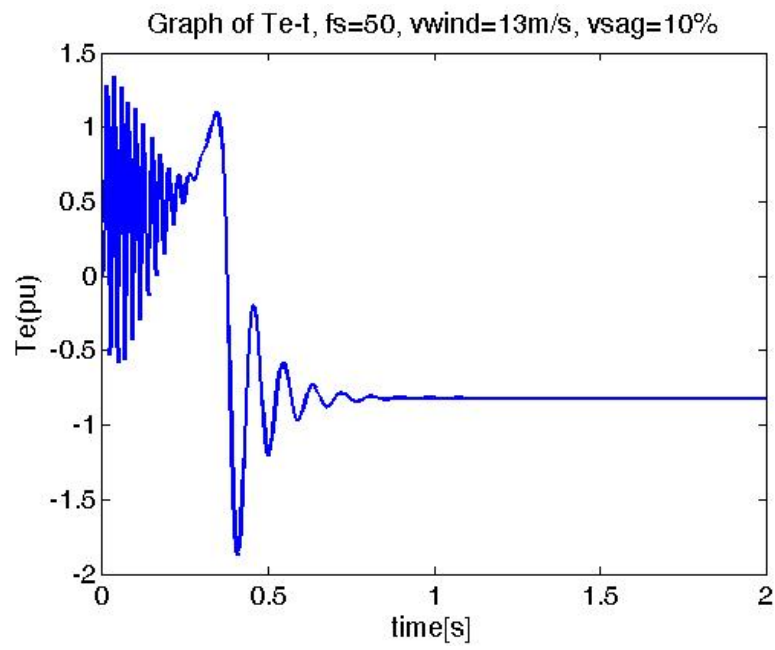


Figure 27. Torque-time in per unit while $V_{sag}=10\%$ and $u_w=13\text{m/s}$, $f_s=50$

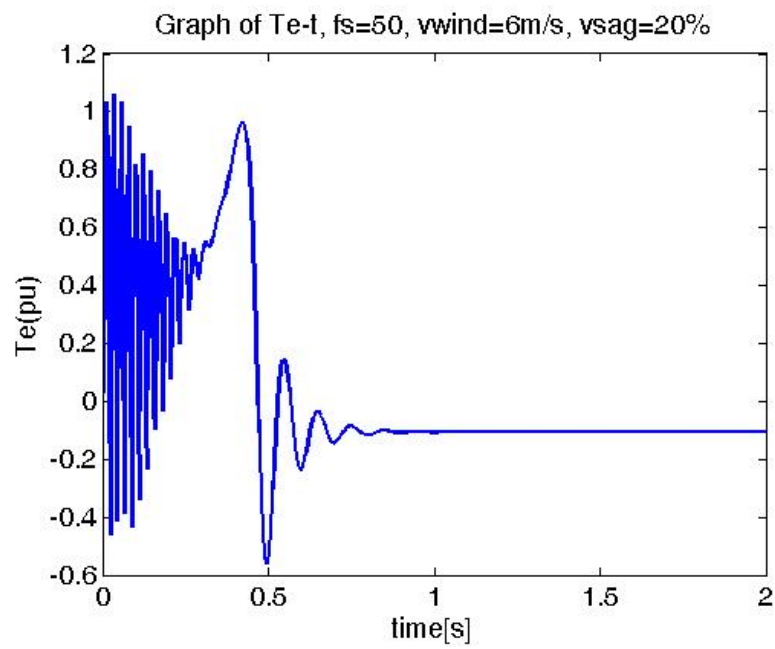


Figure 28. Torque-time in per unit while $V_{sag}=20\%$ and $u_w=6\text{m/s}$, $f_s=50$

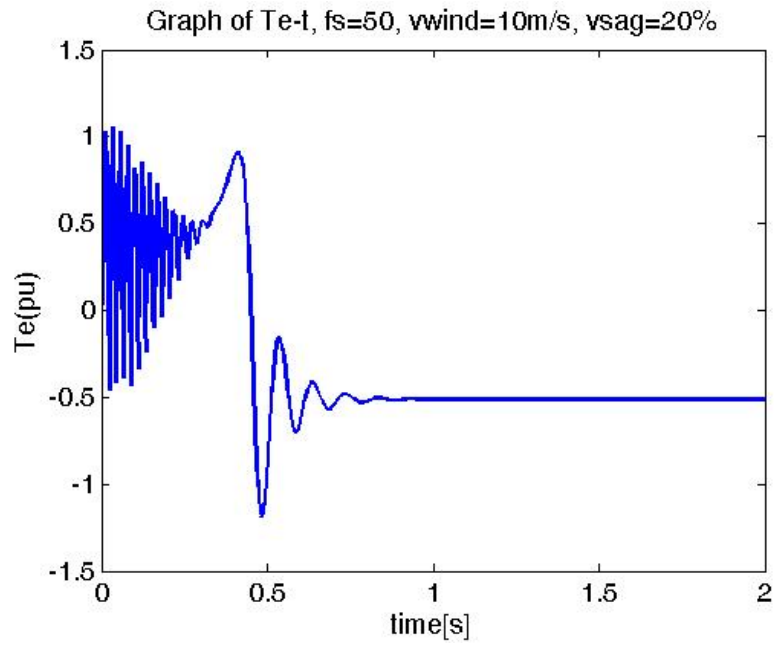


Figure 29. Torque-time in per unit while $V_{sag}=20\%$ and $u_w = 10\text{m/s}$, $f_s = 50$

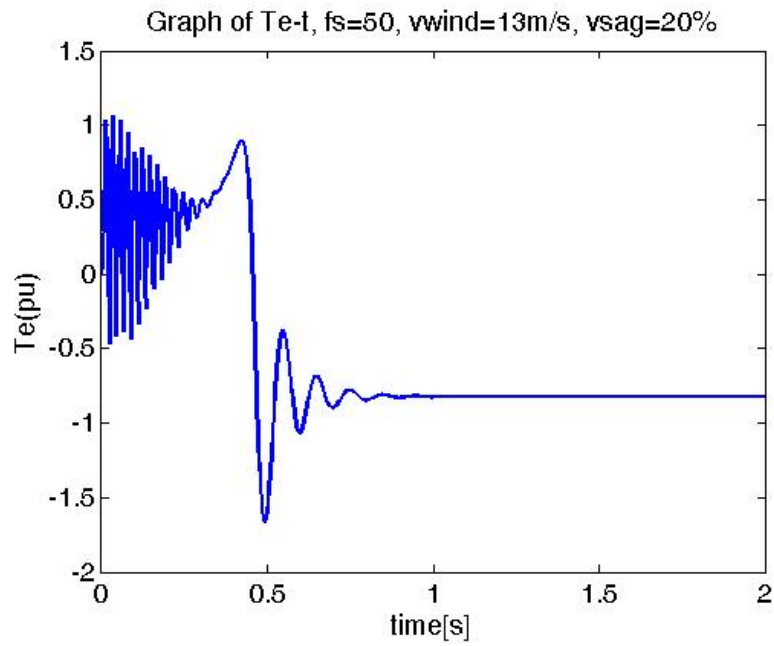


Figure 30. Torque-time in per unit while $V_{sag}=20\%$ and $u_w = 13\text{m/s}$, $f_s = 50$

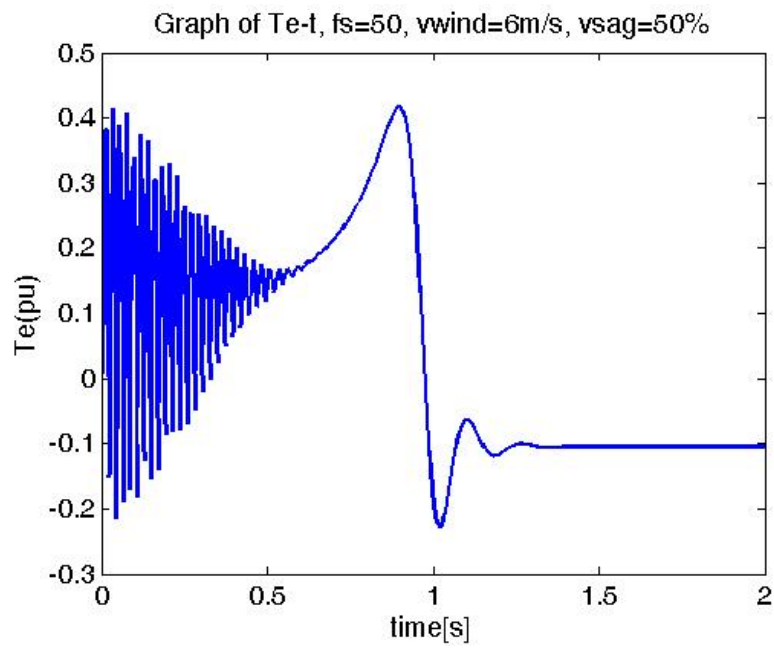


Figure 31. Torque-time in per unit while $V_{sag}=50\%$ and $u_w=6\text{m/s}$, $f_s=50$

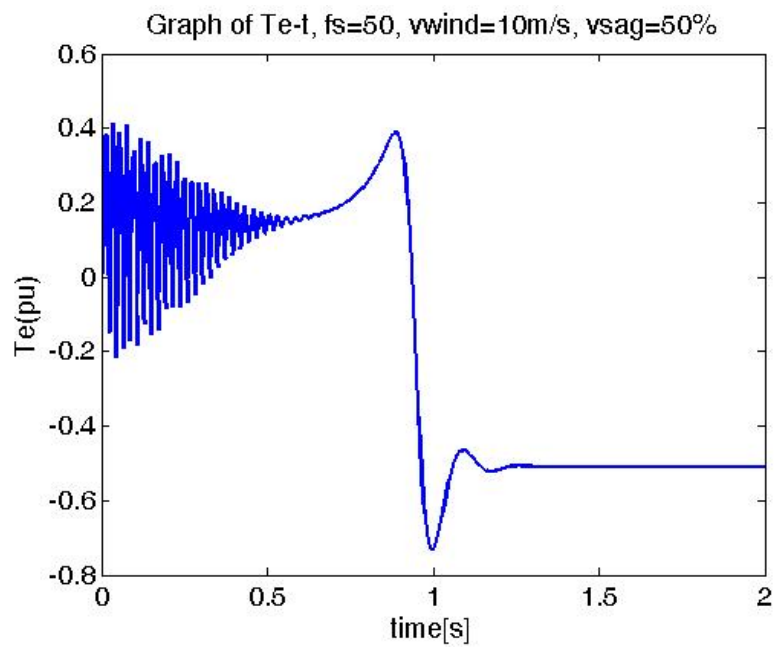


Figure 32. Torque-time in per unit while $V_{sag}=50\%$ and $u_w=10\text{m/s}$, $f_s=50$

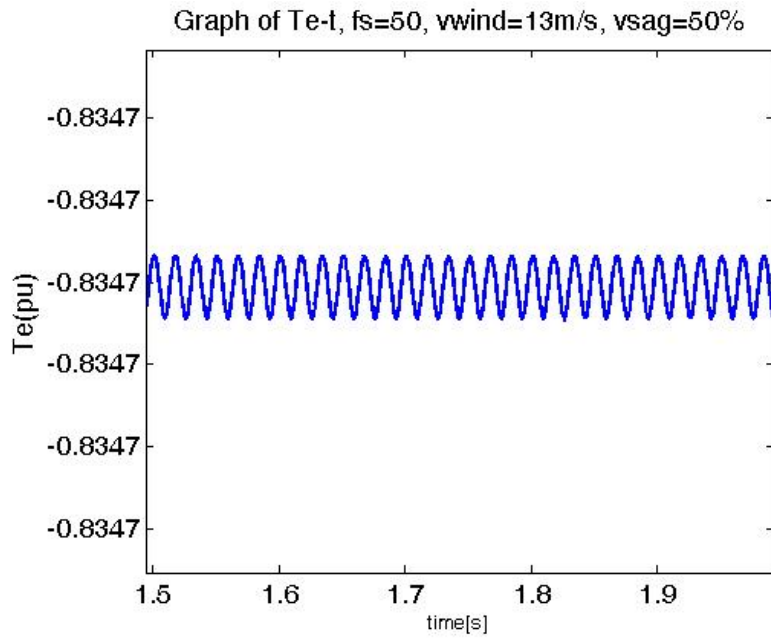


Figure 33. Torque-time in per unit while $V_{sag}=50\%$ and $u_w=13\text{m/s}$, $f_s=50$ in new simulation of wind generator

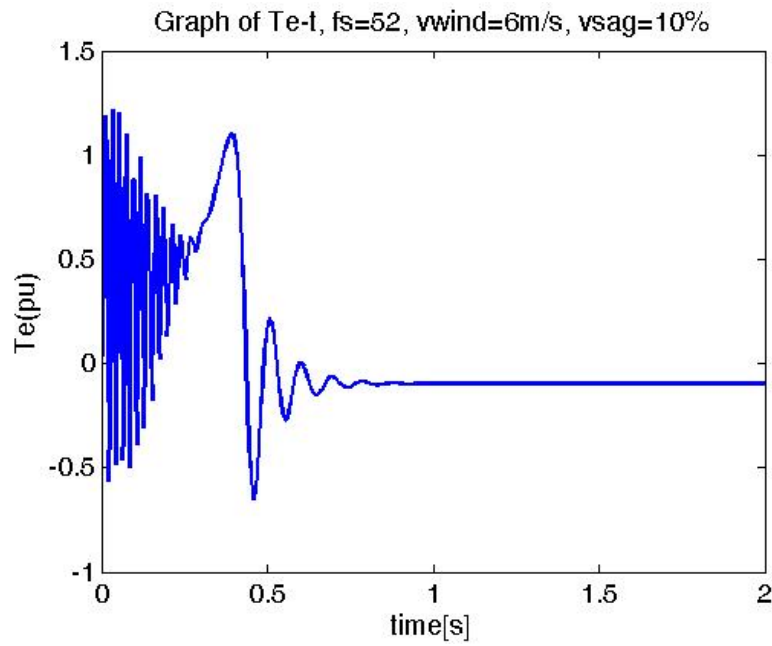


Figure 34. Torque-time in per unit while $V_{sag}=10\%$ and $u_w=6\text{m/s}$, $f_s=52$

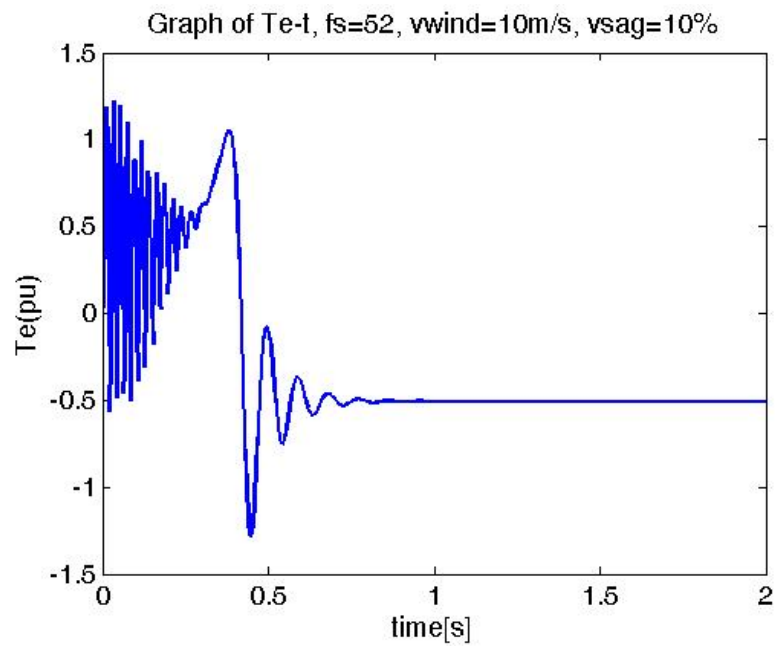


Figure 35. Torque-time in per unit while $V_{sag}=10\%$ and $u_w = 10\text{m/s}$, $f_s = 52$

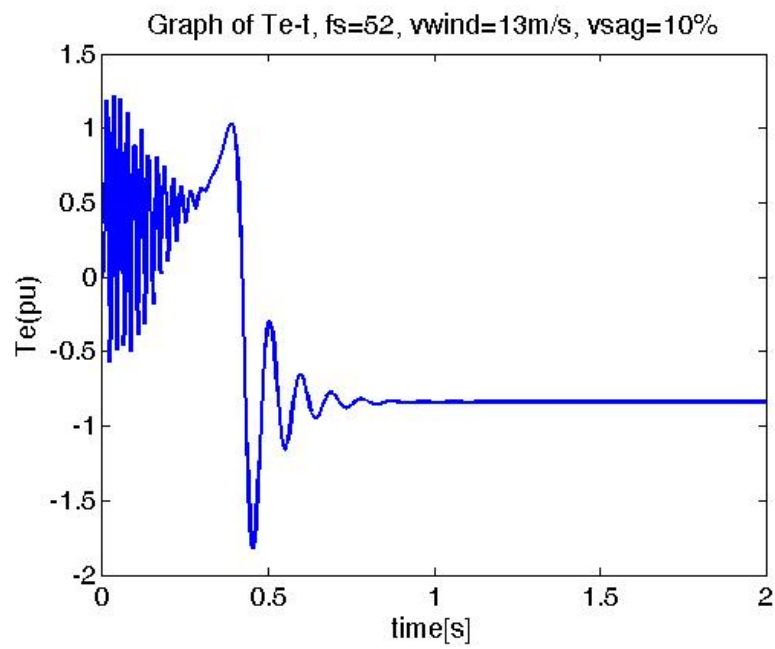


Figure 36. Torque-time in per unit while $V_{sag} = 10\%$ and $u_w = 13\text{m/s}$, $f_s = 52$

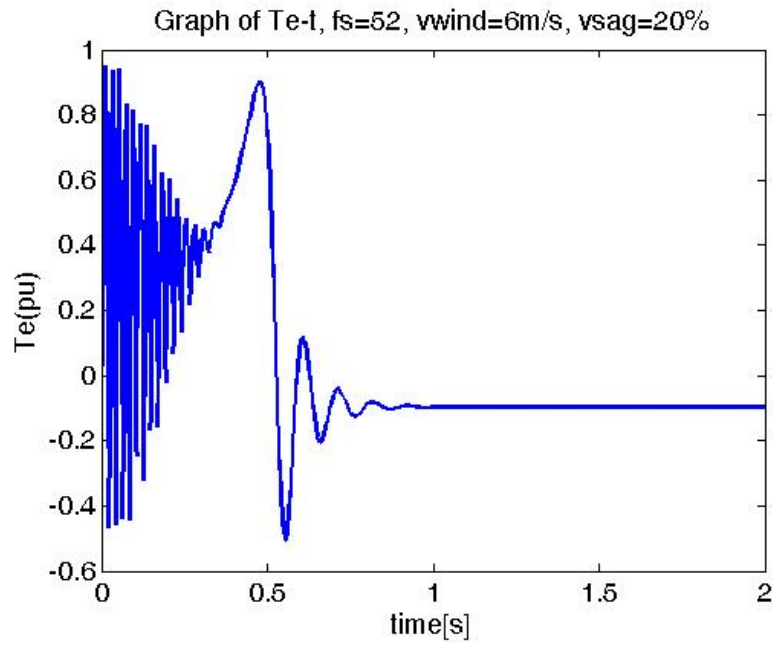


Figure 37. Torque-time in per unit while $V_{sag} = 20\%$ and $u_w = 6\text{m/s}$, $f_s = 52$

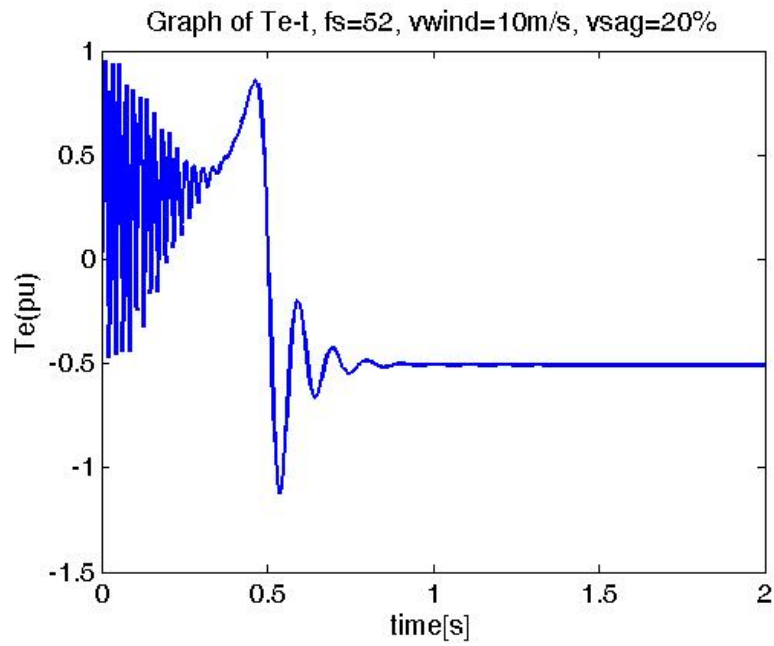


Figure 38. Torque-time in per unit while $V_{sag} = 20\%$ and $u_w = 10\text{m/s}$, $f_s = 52$

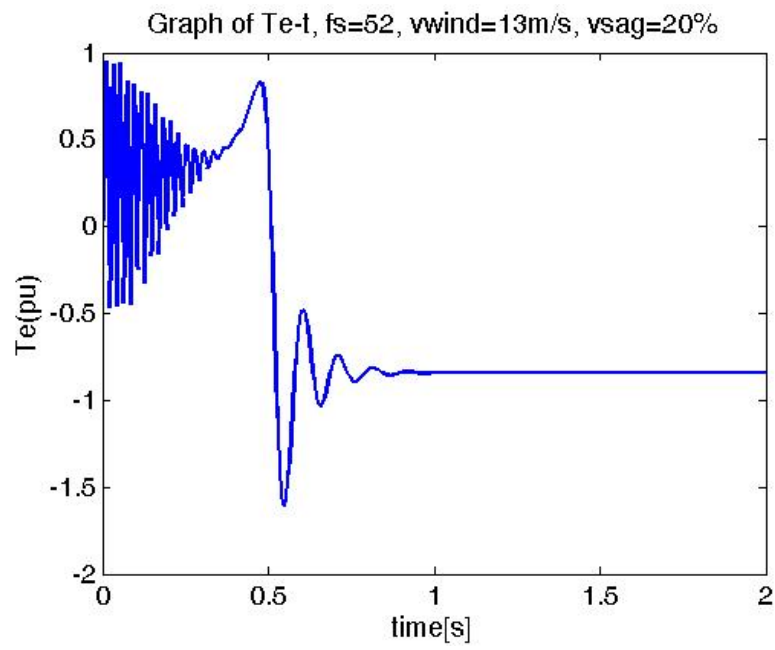


Figure 39. Torque-time in per unit while $V_{sag}=20\%$ and $u_w=13\text{m/s}$, $f_s=52$

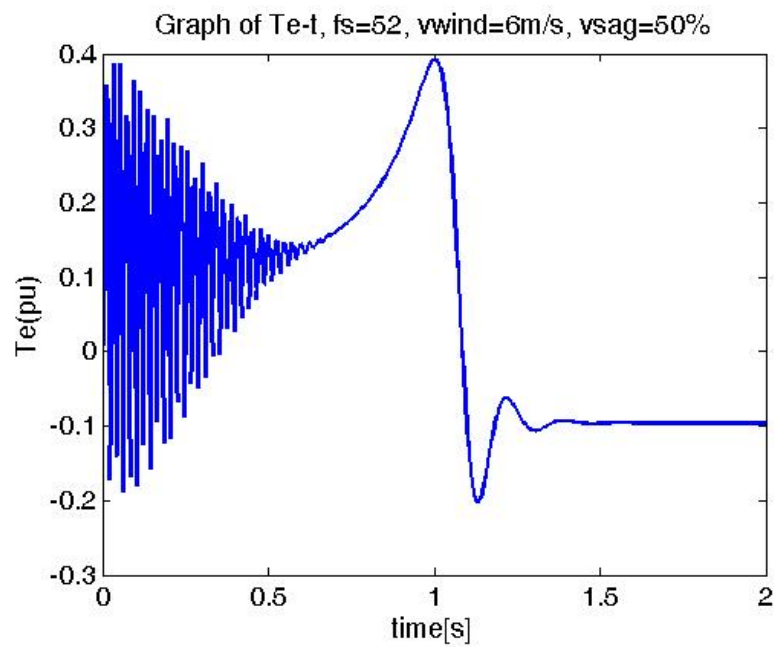


Figure 40. Torque-time in per unit while $V_{sag}=50\%$ and $u_w=6\text{m/s}$, $f_s=52$

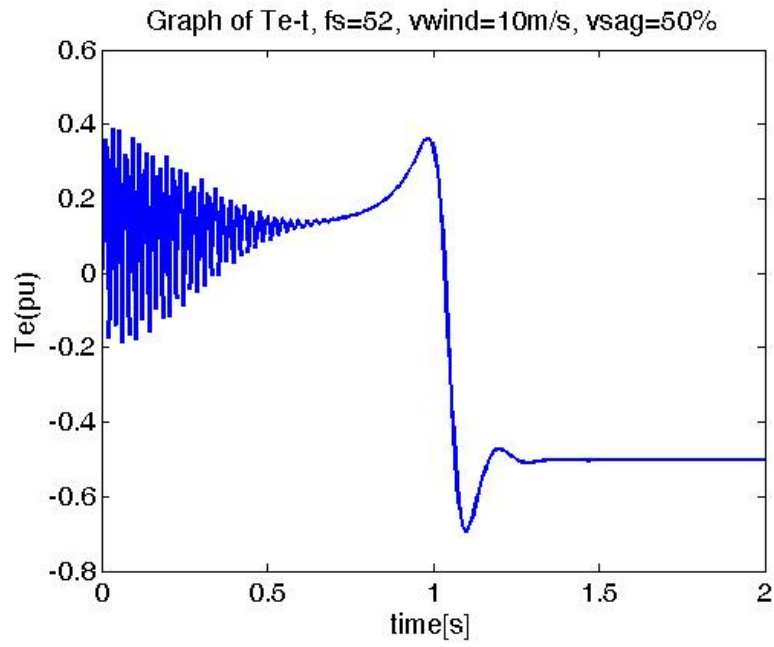


Figure 41. Torque-time in per unit while $V_{sag} = 50\%$ and $u_w = 10\text{m/s}$, $f_s = 52$

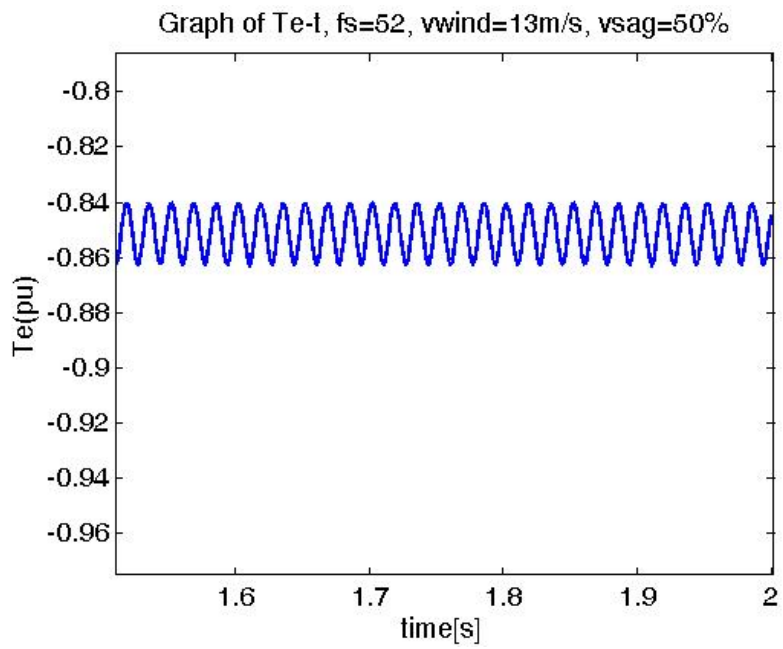


Figure 42. Torque-time in per unit while $V_{sag} = 50\%$ and $u_w = 13\text{m/s}$, $f_s = 52$ in new simulation of wind generator

8. New Simulation of Induction Machine

Figs. 33 and 42 show the results of new simulation of the induction machine model illustrated in Fig. 43 [1]. The new simulation, which has no limiters and switches, is used because at high grid voltage drop-down or sag, the Simulink induction model does not yield realistic results.

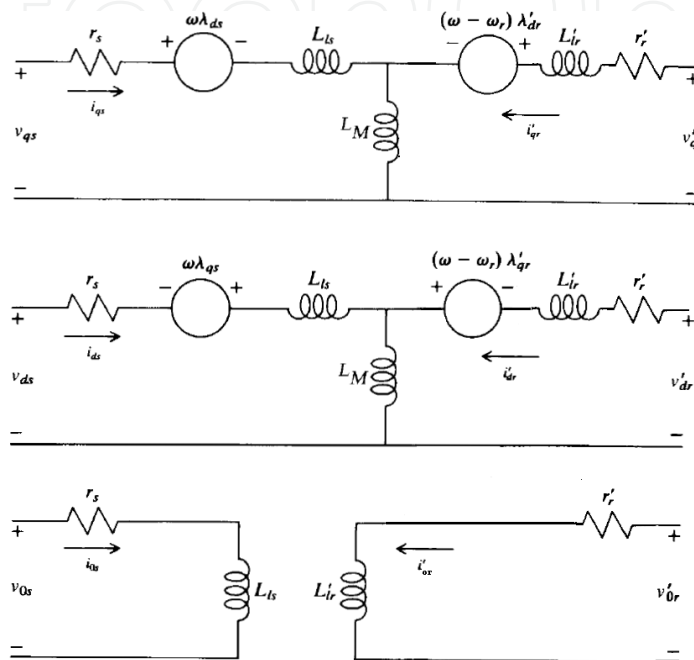


Figure 43. Induction machine Model in dqo system

The new simulation of induction machine is in dqo system and synchronous reference frame simulation on the stator side; n (Transfer coefficient) is assumed to be 1. Circuit theory is used in this simulation, and it does not have saturation and switch blocks, unlike the MATLAB-SIMULINK Induction block. In Fig. 43, L_M is the magnetic mutual inductance, and r and L are the ohm resistance and self-inductance of the dqo circuits, respectively. The machine torque is given by equation (19). In this equation, $i_{d,qs}$ and $\lambda_{d,qs}$ the current and flux parameters, respectively, are derived from linear equations (20)–(23); they are sinusoidal because the voltage sources are sinusoidal.

$$T_e = \left(\frac{3}{2}\right) \left(\frac{P}{2}\right) (\lambda_{ds} i_{qs} - \lambda_{qs} i_{ds}) \quad (19)$$

Where P is poles number, λ_{ds} and λ_{qs} are flux linkages and leakages, respectively, and i_{qs} and i_{ds} are stator currents in q and d circuits of dqo system, respectively.

Then i matrix produced by the λ matrix is given by equation (20).

$$\begin{bmatrix} \lambda_{qdos} \\ \lambda'_{qdor} \end{bmatrix} = \begin{bmatrix} K_s L_s (K_s)^{-1} & K_s L'_{sr} (K_r)^{-1} \\ K_r (L'_{sr})^T (K_s)^{-1} & K_r L'_r (K_r)^{-1} \end{bmatrix} \begin{bmatrix} i_{qdos} \\ i'_{qdor} \end{bmatrix} \quad (20)$$

where the inductance matrix parameters are given by (21), (22), (23).

$$K_s L_s (K_s)^{-1} = \begin{bmatrix} L_{ls} + L_M & 0 & 0 \\ 0 & L_{ls} + L_M & 0 \\ 0 & 0 & L_{ls} \end{bmatrix} \quad (21)$$

$$K_r L'_r (K_r)^{-1} = \begin{bmatrix} L'_{lr} + L_M & 0 & 0 \\ 0 & L'_{lr} + L_M & 0 \\ 0 & 0 & L'_{lr} \end{bmatrix} \quad (22)$$

$$K_s L'_{sr} (K_r)^{-1} = K_r (L'_{sr})^T (K_s)^{-1} = \begin{bmatrix} L_M & 0 & 0 \\ 0 & L_M & 0 \\ 0 & 0 & 0 \end{bmatrix} \quad (23)$$

The linkage and leakage fluxes are given by (24) to (29).

$$\lambda_{qs} = L_{ls} i_{qs} + L_M (i_{qs} + i'_{qr}) \quad (24)$$

$$\lambda_{ds} = L_{ls} i_{ds} + L_M (i_{ds} + i'_{dr}) \quad (25)$$

$$\lambda_{os} = L_{ls} i_{os} \quad (26)$$

$$\lambda'_{qr} = L'_{lr} i'_{qr} + L_M (i_{qs} + i'_{qr}) \quad (27)$$

$$\lambda'_{dr} = L'_{lr} i'_{dr} + L_M (i_{ds} + i'_{dr}) \quad (28)$$

$$\lambda'_{or} = L'_{lr} i'_{or} \quad (29)$$

To create the torque in equation (19), it is necessary to determine the currents in equations (30)–(33) from the stator and rotor currents by using current meters.

$$v_{qs} = r_s i_{qs} + \omega \lambda_{ds} + \frac{d\lambda_{qs}}{dt} \quad (30)$$

$$v_{ds} = r_s i_{ds} - \omega \lambda_{qs} + \frac{d\lambda_{ds}}{dt} \quad (31)$$

$$v'_{qr} = r'_r i'_{qr} + (\omega - \omega_r) \lambda'_{dr} + \frac{d\lambda'_{qr}}{dt} \quad (32)$$

$$v'_{dr} = r'_r i'_{dr} - (\omega - \omega_r) \lambda'_{qr} + \frac{d\lambda'_{dr}}{dt} \quad (33)$$

9. Conclusion

As frequency changes and voltage sag occurs because of turbulence in wind stations in ride-through faults, the system's set point changes. The theoretical and simulation results are similar for one mass shaft and two mass shaft turbine models. At lower wind speeds; 6 and 10 m/s, the directions of the changes in the new working point are the same as those of the frequency changes. At a higher wind speed; 13 m/s, the directions of these changes are opposite to the direction of the frequency changes. Simulation results of high grid voltage sag with SIMULINK induction block has error and new simulation of wind induction generator in synchronous reference frame is presented without error and in 50% voltage sag, new simulation of wind generator model has higher precision than that in 10% and 20% voltage sags; however, this model can simulate wind generator turbulence with voltage sags higher than 50%. Although results of new simulation of induction machine with wind turbine for 50% voltage sag and frequencies 50 and 52 have been presented in this chapter.

10. Nomenclature

P = Generator power

ρ = Air density

A = Turbine rotor area

C_p = Power Coefficient

v_w = Wind speed

θ_{pitch} = Pitch angle

T_e = Electrical torque

T_m = Mechanical torque

J = Inertia

ω_m = Mechanical speed

C = Drag coefficient

ν = Gear box ratio

R = Blade radius

R_s = Stator resistance

L_s = Stator inductance

L_m = Mutual inductance

L'_r = Rotor inductance

R'_r = Rotor resistance

p = Pole pairs

κ = Stiffness

$\lambda_{r,s}$ = Rotor and stator flux

$K_{r,s}$ = Rotor and stator park transformation in synchronous reference frame

$i_{r,s}$ = Rotor and stator current

$v_{r,s}$ = Rotor and stator voltage

11. Future Work

The new simulation of induction generator will be tested by new innovative rain turbine theory and model of the author.

Acknowledgements

I appreciate Dr. Oriol Gomis Bellmunt for conceptualization, Discussions and new information and Dr. Andreas Sumper for discussions about first part of chapter, with special thanks to Dr. Joaquin Pedra for checking reference frame and starting point in new simulation of induction machine.

Author details

Hengameh Kojooyan Jafari*

Address all correspondence to: kojooyan@iiu.ac.ir

Department of Electrical Engineering, Islamic Azad University, Islamshahr Branch, Iran

References

- [1] Krause, Paul C. (1986). Analysis of Electric Machinery. McGraw-Hill, Inc.
- [2] Sunmper, A., Gomis-Bellmunt, O., Sudria-Andreu, A., et al. (2009). Response of Fixed Speed Wind Turbines to System Frequency Disturbances. *IEEE Transaction on Power Systems*, 24(1), 181-192.
- [3] Junyent-Ferre, A., Gomis-Bellmunt, O., Sunmper, A., et al. (2010). Modeling and control of the doubly fed induction generator wind turbine. *Simulation modeling practice and theory journal of ELSEVIER*, 1365-1381.
- [4] Lubosny, Z. (2003). Wind Turbine operation in electric power systems. *Springer publisher*.

IntechOpen

IntechOpen